ELSEVIER

International Journal of Solids and Structures 41 (2004) 5247–5263

INTERNATIONAL JOURNAL OF SOLIDS and STRUCTURES

www.elsevier.com/locate/ijsolstr

Exact three-dimensional solutions of laminated orthotropic piezoelectric rectangular plates featuring interlaminar bonding imperfections modeled by a general spring layer

W.Q. Chen [a,b,*], J.B. Cai [a], G.R. Ye [a], Y.F. Wang [c]

[a] *Department of Civil Engineering, Zhejiang University, Zheda Road 38, Hangzhou 310027, PR China*
[b] *State Key Lab of CAD & CG, Zhejiang University, Hangzhou 310027, PR China*
[c] *Hangzhou Radio and TV University, Hangzhou 310012, PR China*

Received 20 July 2003; received in revised form 8 March 2004
Available online 24 April 2004

Abstract

The bending and free vibration of an imperfectly bonded orthotropic piezoelectric rectangular laminates are investigated using a three-dimensional state-space approach. The plate is assumed to have simple supports only, which enables us to obtain a solution in a completely exact form. A general spring layer is adopted to model the bonding imperfections. The laminated plate that is in a state of cylindrical bending is also considered as a particular case. Numerical results are presented and some particular issues are discussed.

Keywords: Orthotropic piezoelectric material; Laminated rectangular plate; Bonding imperfection; State-space approach; Spring layer model

1. Introduction

Piezoelectric materials and structures have been extensively used in engineering industries and high-tech areas due to their intelligent ability of sensing, actuating and controlling. A large amount of publications on piezoelectric plates and shells can be found (e.g., Tzou, 1993; Rogacheva, 1994; Tani et al., 1998; Wang and Yang, 2000; Ding and Chen, 2001; Fernandes and Pouget, 2002; Altay and Dökmeci, 2003 etc., and the references cited therein). However, little work has been done on laminated piezoelectric plates and shells with imperfect interfaces. On the other hand, laminated elastic structures featuring interlaminar bonding imperfections have been of intense research interest recently (Liu et al., 1994; Cheng et al., 1996a,b, 2000a; Librescu and Schmidt, 2001; Chen and Lee, 2004; Chen et al., 2003, 2004a,b).

* Corresponding author. Tel.: +86-571-879-52284; fax: +86-571-879-52165.
E-mail addresses: chenwq@ccea.zju.edu.cn, chenwq@rocketmail.com (W.Q. Chen).

0020-7683/$ - see front matter © 2004 Elsevier Ltd. All rights reserved.
doi:10.1016/j.ijsolstr.2004.03.010

Multifarious flaws like microcracks, inhomogeneities and voids may be introduced into the bonding layer of a laminated smart structure in the process of manufacture. The bonding strength may also become weakened during the service time of a practical structure. Thus, it is imperative that the effect of imperfect interfaces on the structural behavior should be accurately evaluated. In particular, with the increasing application of piezoelectric actuators and sensors in damage detection of engineering structures, interlaminar debonding in adaptive structures becomes a familiar failure phenomenon and has gained much research interest. Seeley and Chattopadhyay (1999) considered the effect of actuator debonding of adaptive composites using the finite element method. Icardi et al. (2000) presented a dynamic investigation of adaptive cantilever beam with interlayer slips. Zou et al. (2000) made an excellent review on topics related to damage identification and health monitoring for composite structures.

Recently, a three-dimensional exact analysis based on state-space formulations was proposed for a cross-ply rectangular laminate with bonding imperfections described by a spring layer model (Chen et al., 2003). Comparison with the extended zigzag plate theory (Cheng et al., 1996b) showed that although the plate theory is very accurate for perfect laminates, it may become inaccurate when the bonding imperfections are present. Investigation on laminated cylindrical panels also revealed that the high-order shell theory suffers from inaccuracy due to the presence of imperfect interfaces (Chen et al., 2004a). Thus, exact solutions of smart structures featuring interlaminar bonding imperfections become necessary. Moreover, these solutions can also be used as benchmarks for clarifying any two-dimensional plate theories or numerical methods. Wang and Zhong (2003) recently obtained an exact static solution of an infinite imperfect laminated cylindrical shell with surface piezoelectric layers by using a transfer matrix method (Yue and Yin, 1998).

This study extends our previous analysis (Chen et al., 2003) to further take account of the coupling effect between elastic deformation and electric field in a laminated piezoelectric rectangular plate. The analysis is again based on the state-space formulations. It is emphasized here that the state-space approach is very effective in studying laminated structures since the final solving equations always keep the same small scale as that for a single-layered plate (Bahar, 1975). Several works on perfect piezoelectric structures using this approach can be found in literature (Sosa, 1992; Lee and Jiang, 1996; Chen et al., 1997, 1998, 2001; Ding et al., 1999). It will be shown that, compared to the analysis for the perfect laminates, only the so-called interfacial transfer matrices should be integrated into the global transfer matrix.

To describe the imperfection of interlaminar bonding, the general spring layer model is adopted (Aboudi, 1987; Hashin, 1990). It has been widely employed to study the effect of interfacial imperfections on the static and dynamic behavior of laminated structures (Liu et al., 1994; Cheng et al., 1996a,b, 2000a; Icardi et al., 2000). In this paper, in addition to the linear Hooke's relations between mechanical displacements and stress components at the interfaces, a similar relation between the electric potential and electric displacement is further utilized (Fan and Sze, 2001).

In this paper, the problem of a piezoelectric laminate in cylindrical bending is also considered as a particular case.

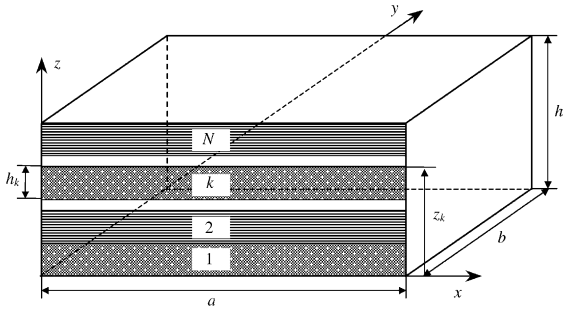

Fig. 1. Geometry of a laminated rectangular plate and the Cartesian coordinates.

2. Basic equations and the state-space approach

Consider an N-layered orthotropic piezoelectric rectangular plate as shown in Fig. 1. The constitutive relations are (Ding and Chen, 2001)

$$\begin{aligned}
&\sigma_x = c_{11}\frac{\partial u}{\partial x} + c_{12}\frac{\partial v}{\partial y} + c_{13}\frac{\partial w}{\partial z} + e_{31}\frac{\partial \phi}{\partial z},\\
&\sigma_y = c_{12}\frac{\partial u}{\partial x} + c_{22}\frac{\partial v}{\partial y} + c_{23}\frac{\partial w}{\partial z} + e_{32}\frac{\partial \phi}{\partial z},\\
&\sigma_z = c_{13}\frac{\partial u}{\partial x} + c_{23}\frac{\partial v}{\partial y} + c_{33}\frac{\partial w}{\partial z} + e_{33}\frac{\partial \phi}{\partial z},\\
&\tau_{yz} = c_{44}\left(\frac{\partial v}{\partial z} + \frac{\partial w}{\partial y}\right) + e_{24}\frac{\partial \phi}{\partial y}, \tau_{xz} = c_{55}\left(\frac{\partial u}{\partial z} + \frac{\partial w}{\partial x}\right) + e_{15}\frac{\partial \phi}{\partial x},\\
&\tau_{xy} = c_{66}\left(\frac{\partial u}{\partial y} + \frac{\partial v}{\partial x}\right), \quad D_x = e_{15}\left(\frac{\partial u}{\partial z} + \frac{\partial w}{\partial x}\right) - \varepsilon_{11}\frac{\partial \phi}{\partial x},\\
&D_y = e_{24}\left(\frac{\partial v}{\partial z} + \frac{\partial w}{\partial y}\right) - \varepsilon_{22}\frac{\partial \phi}{\partial y}, \quad D_z = e_{31}\frac{\partial u}{\partial x} + e_{32}\frac{\partial v}{\partial y} + e_{33}\frac{\partial w}{\partial z} - \varepsilon_{33}\frac{\partial \phi}{\partial z},
\end{aligned} \tag{1}$$

where u, v, and w are the displacement components in x, y, and z-directions, respectively; $\sigma_i(\tau_{ij})$, D_i, and ϕ are the normal (shear) stresses, electric displacements, and electric potential, respectively; and c_{ij}, e_{ij}, and ε_{ij} are the elastic, piezoelectric, and dielectric constants, respectively. The equations of motion in absence of body forces are

$$\begin{aligned}
&\frac{\partial \sigma_x}{\partial x} + \frac{\partial \tau_{xy}}{\partial y} + \frac{\partial \tau_{xz}}{\partial z} = \rho\frac{\partial^2 u}{\partial t^2},\\
&\frac{\partial \tau_{xy}}{\partial x} + \frac{\partial \sigma_y}{\partial y} + \frac{\partial \tau_{yz}}{\partial z} = \rho\frac{\partial^2 v}{\partial t^2},\\
&\frac{\partial \tau_{xz}}{\partial x} + \frac{\partial \tau_{yz}}{\partial y} + \frac{\partial \sigma_z}{\partial z} = \rho\frac{\partial^2 w}{\partial t^2},
\end{aligned} \tag{2}$$

where ρ is the mass density. The equation of electric equilibrium is

$$\frac{\partial D_x}{\partial x} + \frac{\partial D_y}{\partial y} + \frac{\partial D_z}{\partial z} = 0. \tag{3}$$

As shown in Lee and Jiang (1996), Chen et al. (1997, 1998), and Ding and Chen (2001), the following state equation can be directly derived from Eqs. (1) to (3):

$$\frac{\partial}{\partial z}[u, v, \sigma_z, D_z, \tau_{xz}, \tau_{yz}, w, \phi]^{\mathrm{T}} = \mathbf{M}[u, v, \sigma_z, D_z, \tau_{xz}, \tau_{yz}, w, \phi]^{\mathrm{T}}, \tag{4}$$

where the matrix $\mathbf{M}$ is given in Appendix A. Here u, v, w, σ_z, τ_{xz}, τ_{yz}, ϕ, and D_z are termed as state variables, from which the five induced variables σ_x, σ_y, τ_{xy}, D_x, and D_y can be determined from Eq. (A.3).

For the following simply supported boundary conditions (Lee and Jiang, 1996; Ding and Chen, 2001),

$$\begin{aligned}
&\sigma_x = v = w = \phi = 0 \quad \text{at } x = 0, a,\\
&\sigma_y = u = w = \phi = 0 \quad \text{at } y = 0, b,
\end{aligned} \tag{5}$$

we can assume

$$\begin{Bmatrix} u \\ v \\ \sigma_z \\ D_z \\ \tau_{xz} \\ \tau_{yz} \\ w \\ \phi \end{Bmatrix} = \begin{Bmatrix} h\bar{u}(\zeta)\cos(m\pi\xi)\sin(n\pi\eta) \\ h\bar{v}(\zeta)\sin(m\pi\xi)\cos(n\pi\eta) \\ -c_{11}^{(1)}\bar{\sigma}_z(\zeta)\sin(m\pi\xi)\sin(n\pi\eta) \\ -\sqrt{c_{11}^{(1)}\varepsilon_{33}^{(1)}}\overline{D}_z(\zeta)\sin(m\pi\xi)\sin(n\pi\eta) \\ c_{11}^{(1)}\bar{\tau}_{xz}(\zeta)\cos(m\pi\xi)\sin(n\pi\eta) \\ c_{11}^{(1)}\bar{\tau}_{yz}(\zeta)\sin(m\pi\xi)\cos(n\pi\eta) \\ h\bar{w}(\zeta)\sin(m\pi\xi)\sin(n\pi\eta) \\ h\sqrt{c_{11}^{(1)}/\varepsilon_{33}^{(1)}}\bar{\phi}(\zeta)\sin(m\pi\xi)\sin(n\pi\eta) \end{Bmatrix} \exp(\mathrm{i}\omega t), \tag{6}$$

where $\xi = x/a$, $\eta = y/b$, and $\zeta = z/h$ are dimensionless coordinates; m and n are integers; $c_{11}^{(1)}$ and $\varepsilon_{33}^{(1)}$ etc. represent the material constants of the first layer (the bottom layer), and ω is the circular frequency. It can be shown that the simply supported conditions in Eq. (5) have been satisfied automatically. Substituting Eq. (6) into Eq. (4) yields

$$\frac{\mathrm{d}}{\mathrm{d}\zeta}\mathbf{V}(\zeta) = \overline{\mathbf{M}}\mathbf{V}(\zeta), \tag{7}$$

where $\mathbf{V}(\zeta) = [\bar{u}(\zeta), \bar{v}(\zeta), \bar{\sigma}_z(\zeta), \overline{D}_z(\zeta), \bar{\tau}_{xz}(\zeta), \bar{\tau}_{yz}(\zeta), \bar{w}(\zeta), \bar{\phi}(\zeta)]^{\mathrm{T}}$, and the constant coefficient matrix $\overline{\mathbf{M}}$ is also presented in Appendix A. The solution to Eq. (7) can be obtained as

$$\mathbf{V}(\zeta) = \exp[\overline{\mathbf{M}}(\zeta - \zeta_{k-1})]\mathbf{V}(\zeta_{k-1}) \quad (\zeta_{k-1} \leqslant \zeta \leqslant \zeta_k;\ k = 1, 2, \ldots, N), \tag{8}$$

where $\zeta_0 = 0$, $\zeta_k = z_k/h = \sum_{j=1}^{k} h_j/h$, and h_k is the thickness of the kth layer.

Setting $\zeta = \zeta_k$ in Eq. (8), gives

$$\mathbf{V}_1^{(k)} = \mathbf{Q}_k\mathbf{V}_0^{(k)}, \tag{9}$$

where $\mathbf{V}_1^{(k)}$ and $\mathbf{V}_0^{(k)}$ are the state vectors at the upper and lower surfaces, respectively, of the kth layer, and $\mathbf{Q}_k = \exp[\overline{\mathbf{M}}(\zeta_k - \zeta_{k-1})]$ is the transfer matrix of that layer, which can be easily calculated using the built-in functions in MATHEMATIC or MATLAB. Similarly, we get

$$\mathbf{V}_1^{(k+1)} = \mathbf{Q}_{k+1}\mathbf{V}_0^{(k+1)}. \tag{10}$$

3. Imperfect bonding conditions

A general spring-layer model is adopted here to describe the imperfect bonding (Cheng et al., 1996a,b; Fan and Sze, 2001):

$$\begin{aligned} \sigma_z^{(k+1)} &= \sigma_z^{(k)} = K_z^{(k)}[w^{(k+1)} - w^{(k)}], \\ \tau_{xz}^{(k+1)} &= \tau_{xz}^{(k)} = K_x^{(k)}[u^{(k+1)} - u^{(k)}], \\ \tau_{yz}^{(k+1)} &= \tau_{yz}^{(k)} = K_y^{(k)}[v^{(k+1)} - v^{(k)}], \\ D_z^{(k+1)} &= D_z^{(k)} = K_e^{(k)}[\phi^{(k+1)} - \phi^{(k)}] \quad \text{at } z = z_k, \end{aligned} \tag{11}$$

where $K_i^{(k)}$ $(i = x, y, z)$ are the bonding stiffness constants of the interface between the kth layer and $(k+1)$th layer, and $K_e^{(k)}$ is the electric spring constant. Detailed discussion on the mechanical relations of the above spring layer model can be found in Cheng et al. (1996a) and Librescu and Schmidt (2001), which is similarly applied to the electric relation.

In view of Eq. (6), Eq. (11) can be expressed as follows:

$$\mathbf{V}_0^{(k+1)} = \mathbf{P}_k \mathbf{V}_1^{(k)}, \tag{12}$$

where $\mathbf{P}_k$, the interfacial transfer matrix (Chen et al., 2003), is defined as

$$\mathbf{P}_k = \begin{bmatrix} 1 & 0 & 0 & 0 & R_x^{(k)} & 0 & 0 & 0 \\ 0 & 1 & 0 & 0 & 0 & R_y^{(k)} & 0 & 0 \\ 0 & 0 & 1 & 0 & 0 & 0 & 0 & 0 \\ 0 & 0 & 0 & 1 & 0 & 0 & 0 & 0 \\ 0 & 0 & 0 & 0 & 1 & 0 & 0 & 0 \\ 0 & 0 & 0 & 0 & 0 & 1 & 0 & 0 \\ 0 & 0 & -R_z^{(k)} & 0 & 0 & 0 & 1 & 0 \\ 0 & 0 & 0 & -R_e^{(k)} & 0 & 0 & 0 & 1 \end{bmatrix}, \tag{13}$$

where $R_i^{(k)} = c_{11}^{(1)}/[K_i^{(k)} h]$ $(i = x, y, z)$, and $R_e^{(k)} = \varepsilon_{33}^{(1)}/[K_e^{(k)} h]$ are dimensionless compliance coefficients of the interfaces.

From Eqs. (9), (10) and (12), a relation between the state vector at the upper surface of the $(k+1)$th layer and that at the lower surface of the kth layer is established as

$$\mathbf{V}_1^{(k+1)} = \mathbf{Q}_{k+1} \mathbf{P}_k \mathbf{Q}_k \mathbf{V}_0^{(k)}. \tag{14}$$

Continuing the above procedure, leads to the relation between the state vectors at the top and bottom surfaces of the laminate

$$\mathbf{V}_1^{(N)} = \mathbf{T} \mathbf{V}_0^{(1)}, \tag{15}$$

where $\mathbf{T} = (\prod_{j=N}^{2} \mathbf{Q}_j \mathbf{P}_{j-1}) \mathbf{Q}_1$ is the global transfer matrix for a laminated orthotropic piezoelectric plate featuring interfacial bonding imperfections. In case of a perfectly bonded plate, all $\mathbf{P}_j$ become unit, and we have $\mathbf{T} = \prod_{j=N}^{1} \mathbf{Q}_j$ (Ding and Chen, 2001).

4. Bending and free vibration analysis

Consider the bending problem ($\omega = 0$) of a plate subjected to generally distributed normal pressures $p(x, y)$ and $q(x, y)$ on the bottom and top surfaces, respectively. These loads can be expanded in terms of double sine functions as follows:

$$\begin{aligned} p(x,y) &= c_{11}^{(1)} \sum_{m=1}^{\infty} \sum_{n=1}^{\infty} a_{mn} \sin(m\pi\xi) \sin(n\pi\eta), \\ q(x,y) &= c_{11}^{(1)} \sum_{m=1}^{\infty} \sum_{n=1}^{\infty} b_{mn} \sin(m\pi\xi) \sin(n\pi\eta), \end{aligned} \tag{16}$$

where $[a_{mn}, b_{mn}] = [4/c_{11}^{(1)}] \int_0^1 \int_0^1 [p(\xi,\eta), q(\xi,\eta)] \sin(m\pi\xi) \sin(n\pi\eta)\, \mathrm{d}\xi\, \mathrm{d}\eta$. For an arbitrary couple of (m, n), the surface mechanical boundary conditions are

$$\bar{\sigma}_z(0) = a_{mn}, \quad \bar{\sigma}_z(1) = b_{mn}, \quad \bar{\tau}_{xz}(1) = \bar{\tau}_{yz}(1) = \bar{\tau}_{xz}(0) = \bar{\tau}_{yz}(0) = 0. \tag{17}$$

On the other hand, there are two types of electric conditions frequently encountered in practice, i.e. the open-circuit and closed-circuit conditions:

$$\text{Open:} \quad \overline{D}_z(0) = \overline{D}_z(1) = 0, \qquad \text{Closed:} \quad \bar{\phi}(0) = \bar{\phi}(1) = 0. \tag{18}$$

Thus we can obtain from Eq. (15)

$$\begin{Bmatrix} \bar{u}(0) \\ \bar{v}(0) \\ \bar{w}(0) \\ \bar{\phi}(0) \end{Bmatrix} = \begin{bmatrix} T_{31} & T_{32} & T_{37} & T_{38} \\ T_{41} & T_{42} & T_{47} & T_{48} \\ T_{51} & T_{52} & T_{57} & T_{58} \\ T_{61} & T_{62} & T_{67} & T_{68} \end{bmatrix}^{-1} \begin{Bmatrix} b_{mn} - T_{33}a_{mn} \\ -T_{43}a_{mn} \\ -T_{53}a_{mn} \\ -T_{63}a_{mn} \end{Bmatrix} \tag{19}$$

for the open-circuit electric condition, and

$$\begin{Bmatrix} \bar{u}(0) \\ \bar{v}(0) \\ \overline{D}_z(0) \\ \bar{w}(0) \end{Bmatrix} = \begin{bmatrix} T_{31} & T_{32} & T_{34} & T_{37} \\ T_{51} & T_{52} & T_{54} & T_{57} \\ T_{61} & T_{62} & T_{64} & T_{67} \\ T_{81} & T_{82} & T_{84} & T_{87} \end{bmatrix}^{-1} \begin{Bmatrix} b_{mn} - T_{33}a_{mn} \\ -T_{53}a_{mn} \\ -T_{63}a_{mn} \\ -T_{83}a_{mn} \end{Bmatrix} \tag{20}$$

for the closed-circuit condition. In Eqs. (19) and (20) T_{ij} represents the elements of matrix $\mathbf{T}$. The state vector for any value of ζ can then be determined by

$$\mathbf{V}(\zeta) = \exp[\overline{\mathbf{M}}(\zeta - \zeta_{k-1})] \left(\prod_{j=k-1}^{1} \mathbf{Q}_j \mathbf{P}_{j-1} \right) \mathbf{V}_0^{(1)} \quad (\zeta_{k-1} \leqslant \zeta \leqslant \zeta_k;\ k = 1, 2, \ldots, N), \tag{21}$$

where $\mathbf{P}_0$ is an 8th-order identity matrix.

Now consider the free vibration problem. If the plate is traction-free at the top and bottom surfaces, the following frequency equations can be derived:

$$\begin{vmatrix} T_{31} & T_{32} & T_{37} & T_{38} \\ T_{41} & T_{42} & T_{47} & T_{48} \\ T_{51} & T_{52} & T_{57} & T_{58} \\ T_{61} & T_{62} & T_{67} & T_{68} \end{vmatrix} = 0 \tag{22}$$

for the open-circuit condition, and

$$\begin{vmatrix} T_{31} & T_{32} & T_{34} & T_{37} \\ T_{51} & T_{52} & T_{54} & T_{57} \\ T_{61} & T_{62} & T_{64} & T_{67} \\ T_{81} & T_{82} & T_{84} & T_{87} \end{vmatrix} = 0 \tag{23}$$

for the closed-circuit condition.

It is known that when $b \to \infty$, the plate will be in a state of cylindrical bending, for which only two displacements u and w, in x and z directions, respectively are non-zero, and both are independent of the coordinate y. The corresponding state equation is given in Eq. (A.6) in Appendix A, and the analysis is very similar to those presented above, which is omitted here for brevity.

5. Numerical examples

In all examples to be considered, we assume $R_z^{(k)} = 0$ to avoid the material penetration phenomenon (Cheng et al., 1996a,b). Note that the delamination problem of a laminated plate subjected to static normal tension loads, i.e. upward at the top surface and downward at the bottom surface, can be considered by

taking $R_z^{(k)} \neq 0$ (Shu and Soldatos, 2001). We also take $R_x^{(k)} = R_y^{(k)} = R_e^{(k)} = R^{(k)}$ for simplicity. In addition, each layer in the laminate is considered to have the same thickness.

First, consider the free vibration of a simply supported four layered PZT-4/PVDF/PVDF/PZT-4 square plate, with the PVDF layer oriented at 0° with respect to the x-axis. Only in this example, the material constants in Heyliger and Saravanos (1995), which are listed in Table 1 for readers' convenience, are employed for comparison purpose.

The six lowest non-dimensional frequencies $\Omega = \omega h\sqrt{\rho^{(1)}/c_{11}^{(1)}}$ are given in Table 2 with $R^{(1)} = 0.5R^{(2)} = R^{(3)} = R$ being employed. The results for the perfect laminate, when transformed to the frequency parameter $\omega/100$, are found identical to those obtained by Heyliger and Saravanos (1995). It is shown that with the increase of R, the frequency of the laminate decreases, due to the reduction of plate's rigidity that is induced by the interfacial imperfections.

We notice here that, like the elastic plate (Chen et al., 2003), the sensitivity of frequency to the interfacial imperfection depends greatly on the frequency order. For example, the relative error defined by $(\omega|_{R=0.6} - \omega|_{R=0})/\omega|_{R=0}$, for the first lowest natural frequency is only about -0.1% when $a/h = 50$, while it becomes -6% or so for the fifth frequency, for both types of electric conditions. This property is very important in practice because one can consciously select for consideration the vibrational modes whose frequencies vary significantly with the interfacial flaws. This can improve the reliability and precision of evaluation of engineering structures.

The lowest frequency parameters $\Omega^* = 100\omega h\sqrt{\rho^{(1)}/c_{11}^{(1)}}$ of rectangular PVDF laminates with $a/h = 10$ are given in Table 3 for several different layup schemes. In this example, we assume a uniform imperfection, i.e. $R^{(1)} = R^{(2)} = \cdots R^{(N)} = R$. Hereafter, the material constants of PVDF and PZT-4 in Cheng et al. (2000b) are adopted, which are also listed in Table 1. The formulations for the laminate in cylindrical bending are directly employed to calculate the results for $b/h \to \infty$. Just as the elastic case, the frequencies of the rectangular laminate converge rapidly to that of the laminate in cylindrical bending when b/a increases. In fact, the lowest natural frequency of the rectangular laminate of $b/a = 5$ has a relative error smaller than

Table 1
Material constants of PZT-4 and PVDF[a]

Property	Heyliger and Saravanos (1995)		Property	Cheng et al. (2000b)	
	PZT-4	PVDF		PZT-4	PVDF
E_1 (GPa)	81.3	237.0	c_{11} (GPa)	139	238.24
E_2 (GPa)	81.3	23.2	c_{22} (GPa)	139	23.6
E_3 (GPa)	64.5	10.5	c_{33} (GPa)	115	10.64
ν_{12}	0.329	0.154	c_{12} (GPa)	77.8	3.98
ν_{13}	0.432	0.178	c_{13} (GPa)	74.3	2.19
ν_{23}	0.432	0.177	c_{23} (GPa)	74.3	1.92
G_{23} (GPa)	25.6	2.15	c_{44} (GPa)	25.6	2.15
G_{13} (GPa)	25.6	4.4	c_{55} (GPa)	25.6	4.4
G_{12} (GPa)	30.6	6.43	c_{66} (GPa)	30.6	6.43
e_{31} (C/m^2)	−5.20	−0.13	e_{31} (C/m^2)	−5.2	−0.13
e_{32} (C/m^2)	−5.20	−0.14	e_{32} (C/m^2)	−5.2	−0.145
e_{33} (C/m^2)	15.08	−0.28	e_{33} (C/m^2)	15.1	−0.276
e_{24} (C/m^2)	12.72	−0.01	e_{24} (C/m^2)	12.7	−0.009
e_{15} (C/m^2)	–[b]	–[b]	e_{15} (C/m^2)	12.7	−0.135
$\varepsilon_{11}/\varepsilon_0$[c]	1475	12.5	$\varepsilon_{11}/\varepsilon_0$[c]	1475	12.5
$\varepsilon_{22}/\varepsilon_0$	1475	11.98	$\varepsilon_{22}/\varepsilon_0$	1475	11.98
$\varepsilon_{33}/\varepsilon_0$	1300	11.98	$\varepsilon_{33}/\varepsilon_0$	1300	11.98

[a] The densities of PZT-4 and PVDF are assumed to be identical, as done in Heyliger and Saravanos (1995).
[b] The value of e_{15} was not given in Heyliger and Saravanos (1995), but use was made of $e_{15} = e_{24}$ in their calculation (Heyliger, 2003).
[c] $\varepsilon_0 = 8.85 \times 10^{-12}$ (F/m) in Heyliger and Saravanos (1995), and $\varepsilon_0 = 8.854185 \times 10^{-12}$ (F/m) in Cheng et al. (2000b).

Table 2
First six non-dimensional frequencies $\left(\Omega = \omega h\sqrt{\rho^{(1)}/c_{11}^{(1)}}\right)$ of a four-ply square laminate ($m = n = 1$)

Electric condition	a/h	R	1	2	3	4	5	6
Open	4	0.0	0.156506	0.516113	0.728854	0.883968	0.976442	1.09364
		0.2	0.154778	0.514975	0.724029	0.882140	0.975443	1.08652
		0.4	0.153133	0.513859	0.719393	0.880264	0.974430	1.07985
		0.6	0.151565	0.512766	0.714937	0.878342	0.973401	1.07359
	50	0.0	0.00194510	0.0440889	0.0765848	0.428759	0.607858	0.975741
		0.2	0.00194445	0.0440880	0.0765842	0.424169	0.594852	0.975513
		0.4	0.00194381	0.0440871	0.0765837	0.419713	0.582596	0.973402
		0.6	0.00194316	0.0440862	0.0765832	0.415386	0.571027	0.966228
Closed	4	0.0	0.156223	0.516037	0.728853	0.883944	0.973696	1.09068
		0.2	0.154501	0.514901	0.724026	0.882115	0.972665	1.08367
		0.4	0.152862	0.513788	0.719390	0.880239	0.971618	1.07712
		0.6	0.151299	0.512697	0.714933	0.878316	0.970554	1.07096
	50	0.0	0.00194504	0.0440657	0.0765329	0.428400	0.606717	0.947783
		0.2	0.00194439	0.0440644	0.0765315	0.423822	0.593781	0.947241
		0.4	0.00194375	0.0440631	0.0765301	0.419377	0.581588	0.946643
		0.6	0.00194310	0.0440617	0.0765287	0.415061	0.570077	0.945944

Table 3
Lowest frequency parameters $\left(\Omega^* = 100\omega h\sqrt{\rho^{(1)}/c_{11}^{(1)}}\right)$ of simply-supported rectangular PVDF laminates with uniform interfacial imperfection ($a/h = 10$, $m = n = 1$)[a]

Stacking sequence[b]	b/h	$R = 0$	$R = 0.2$	$R = 0.4$	$R = 0.6$
[0/90°]	10	6.60800	6.59228	6.57683	6.56164
	50	4.34998	4.34214	4.33441	4.32678
	100	4.31881	4.31107	4.30344	4.29591
	200	4.31171	4.30399	4.29638	4.28887
	300	4.31042	4.30271	4.29510	4.28760
	∞	4.30940	4.30170	4.29409	4.28659
[0/90/0°]	10	2.42954	2.42627	2.42301	2.41977
	50	2.10358	2.10027	2.09697	2.09369
	100	2.09888	2.09556	2.09227	2.08899
	200	2.09776	2.09445	2.09116	2.08788
	300	2.09756	2.09425	2.09096	2.08768
	∞	2.09740	2.09409	2.09079	2.08752
[0/90/0/90°]	10	7.67854	7.55903	7.44595	7.33878
	50	5.21066	5.13375	5.06083	4.99155
	100	5.18333	5.10653	5.03370	4.96452
	200	5.17742	5.10066	5.02786	4.95870
	300	5.17637	5.09962	5.02682	4.95767
	∞	5.17554	5.09879	5.02600	4.95685
[$(0/90)_2$0°]	10	2.51310	2.50768	2.50229	2.49695
	50	2.01755	2.01283	2.00815	2.00350
	100	2.01185	2.00713	2.00246	1.99781
	200	2.01056	2.00585	2.00118	1.99654
	300	2.01033	2.00562	2.00095	1.99631
	∞	2.01015	2.00544	2.00076	1.99612

[a] Open electric condition at both surfaces.
[b] The stacking sequence is from the top to bottom.

1% when compared to that of the laminate in cylindrical bending, either for the perfect case or for the imperfect cases.

Now we turn to consider the bending problem of a three-ply ([0/90/0°]) PVDF laminate in cylindrical bending with a uniform interfacial imperfection ($R^{(1)} = R^{(2)} = R$) subjected to a sinusoidal pressure $q = q_0 \sin(\pi\xi)$ applied at the top surface. The closed-circuit electric condition is adopted at both surfaces. Since the present analysis is completely exact, we present the numerical results in Tables 4–12, which can serve as benchmarks for future study using different methods. For the purpose of comparison, the nine field variables are all non-dimensionalized according to Cheng et al. (2000b):

Table 4
Amplitude of in-plane mechanical displacement $\bar{u}_1 \times 10^{10}$ for a three-ply ([0/90/0°]) PVDF laminate in cylindrical bending under sinusoidal mechanical load

ζ	$a/h = 4$				$a/h = 10$			
	$R = 0.0$	$R = 0.2$	$R = 0.4$	$R = 0.6$	$R = 0.0$	$R = 0.2$	$R = 0.4$	$R = 0.6$
0	0.232394	0.232830	0.230608	0.237176	0.968681	0.969761	0.969730	0.973597
0.1	0.118249	0.118231	0.116713	0.120162	0.692871	0.693058	0.692330	0.694815
0.2	0.044356	0.043914	0.042858	0.043848	0.454035	0.453346	0.451923	0.453077
0.3	−0.014791	−0.015771	−0.016446	−0.018107	0.239388	0.237790	0.235636	0.235441
1/3	−0.034788	−0.036001	−0.036544	−0.039283	0.171200	0.169284	0.166871	0.166211
1/3	−0.034788	−0.032871	−0.030336	−0.029891	0.171200	0.172850	0.173996	0.176906
0.4	−0.017320	−0.016186	−0.014679	−0.014430	0.103637	0.104587	0.105006	0.107285
0.5	0.006936	0.006985	0.007274	0.006768	0.002928	0.002840	0.002207	0.003488
0.6	0.029902	0.028909	0.028299	0.026442	−0.098030	−0.099151	−0.100802	−0.100589
2/3	0.045041	0.043344	0.042283	0.039150	−0.166036	−0.167849	−0.170162	−0.170708
2/3	0.045041	0.046455	0.048526	0.048390	−0.166036	−0.164288	−0.163040	−0.160043
0.7	0.023830	0.024899	0.026261	0.026628	−0.234454	−0.233043	−0.232192	−0.229384
0.8	−0.038968	−0.038716	−0.039082	−0.037406	−0.449916	−0.449472	−0.449763	−0.447478
0.9	−0.117503	−0.117942	−0.119880	−0.116849	−0.689790	−0.690285	−0.691694	−0.689890
1	−0.238873	−0.240117	−0.244011	−0.239107	−0.966919	−0.968372	−0.970934	−0.969595

Table 5
Amplitude of transverse mechanical displacement $\bar{u}_3 \times 10^{10}$ for a three-ply ([0/90/0°]) PVDF laminate in cylindrical bending under sinusoidal mechanical load

ζ	$a/h = 4$				$a/h = 10$			
	$R = 0.0$	$R = 0.2$	$R = 0.4$	$R = 0.6$	$R = 0.0$	$R = 0.2$	$R = 0.4$	$R = 0.6$
0	1.854100	1.860678	1.849267	1.897279	9.517795	9.546966	9.569539	9.615148
0.1	1.857581	1.864706	1.857378	1.897753	9.523759	9.553156	9.577262	9.619808
0.2	1.861251	1.868921	1.865701	1.898382	9.528497	9.558113	9.583750	9.623223
0.3	1.866469	1.874685	1.875609	1.900505	9.532625	9.562455	9.589620	9.626005
1/3	1.868622	1.877018	1.879337	1.901606	9.533936	9.563836	9.591510	9.626862
0.4	1.873836	1.882620	1.887750	1.904800	9.536587	9.566640	9.595347	9.628646
0.5	1.884152	1.893497	1.902798	1.912054	9.541026	9.571304	9.601551	9.631768
0.6	1.897425	1.907310	1.920760	1.922202	9.546023	9.576517	9.608298	9.635426
2/3	1.907912	1.918147	1.934371	1.930554	9.549659	9.580295	9.613095	9.638158
0.7	1.913602	1.924026	1.941652	1.935216	9.551493	9.582205	9.615521	9.639559
0.8	1.931883	1.942857	1.964634	1.950419	9.556793	9.587732	9.622590	9.643552
0.9	1.951690	1.963203	1.989079	1.967164	9.561476	9.592635	9.629024	9.646913
1	1.971639	1.983682	2.013625	1.984056	9.564924	9.596297	9.634209	9.649024

Table 6
Amplitude of transverse shear stress $\bar{\tau}_{13}$ for a three-ply ([0/90/0°]) PVDF laminate in cylindrical bending under sinusoidal mechanical load

ζ	$a/h = 4$				$a/h = 10$			
	$R = 0.0$	$R = 0.2$	$R = 0.4$	$R = 0.6$	$R = 0.0$	$R = 0.2$	$R = 0.4$	$R = 0.6$
0	0	0	0	0	0	0	0	0
0.1	1.001178	1.002834	0.995679	1.017665	1.941529	1.943205	1.943672	1.948374
0.2	1.464300	1.465111	1.454160	1.482135	3.281319	3.282602	3.281912	3.288143
0.3	1.545873	1.543098	1.530813	1.550071	4.090574	4.089378	4.085866	4.090490
1/3	1.496079	1.491330	1.479117	1.491713	4.250610	4.248106	4.243265	4.246638
0.4	1.483020	1.479285	1.471130	1.477687	4.270553	4.268418	4.264885	4.266271
0.5	1.473960	1.471211	1.468474	1.465751	4.280400	4.278619	4.276840	4.275063
0.6	1.476639	1.474270	1.476351	1.463748	4.266209	4.264545	4.264283	4.259105
2/3	1.484710	1.482265	1.487317	1.467595	4.243313	4.241595	4.242217	4.234630
0.7	1.548002	1.548146	1.557812	1.535948	4.085072	4.084654	4.086555	4.080321
0.8	1.492833	1.497233	1.513371	1.490558	3.280013	3.281958	3.285874	3.282864
0.9	1.032403	1.036744	1.049868	1.033823	1.942254	1.944334	1.947620	1.946666
1	0	0	0	0	0	0	0	0

Table 7
Amplitude of transverse normal stress $\bar{\tau}_{33}$ for a three-ply ([0/90/0°]) PVDF laminate in cylindrical bending under sinusoidal mechanical load

ζ	$a/h = 4$				$a/h = 10$			
	$R = 0.0$	$R = 0.2$	$R = 0.4$	$R = 0.6$	$R = 0.0$	$R = 0.2$	$R = 0.4$	$R = 0.6$
0	0	0	0	0	0	0	0	0
0.1	0.043681	0.043763	0.043455	0.044438	0.032191	0.032223	0.032235	0.032317
0.2	0.143333	0.143528	0.142491	0.145530	0.115700	0.115783	0.115796	0.116058
0.3	0.263813	0.263952	0.261988	0.266984	0.232817	0.232907	0.232858	0.233299
1/3	0.303718	0.303760	0.301474	0.306892	0.276538	0.276609	0.276517	0.277000
0.4	0.381685	0.381506	0.378689	0.384608	0.365790	0.365813	0.365633	0.366166
0.5	0.497726	0.497296	0.494056	0.500129	0.500171	0.500133	0.499870	0.500398
0.6	0.613521	0.612894	0.609631	0.615107	0.634484	0.634393	0.634098	0.634517
2/3	0.691027	0.690275	0.687200	0.691832	0.723614	0.723488	0.723197	0.723483
0.7	0.730816	0.730035	0.727156	0.731241	0.767268	0.767131	0.766854	0.767067
0.8	0.852641	0.852070	0.850270	0.852550	0.884284	0.884176	0.883997	0.884069
0.9	0.954817	0.954616	0.954025	0.954727	0.967789	0.967750	0.967692	0.967704
1	1	1	1	1	1	1	1	1

$$\bar{u}_1 = \frac{u}{Pa}, \quad \bar{u}_3 = \frac{w}{Pa}, \quad \bar{\tau}_{11} = \frac{\sigma_x}{Pc^*}, \quad \bar{\tau}_{22} = \frac{\sigma_y}{Pc^*}, \quad \bar{\tau}_{33} = \frac{\sigma_z}{Pc^*},$$
$$\bar{\tau}_{13} = \frac{\tau_{xz}}{Pc^*}, \quad \bar{\varphi} = \frac{\phi e^*}{Pac^*}, \quad \overline{D}_1 = \frac{D_x}{Pe^*}, \quad \overline{D}_3 = \frac{D_z}{Pe^*}, \tag{24}$$

where $P = -q_0/c^*$ with $c^* = 1\ \mathrm{N/m^2}$ and $e^* = 1\ \mathrm{C/m^2}$.

It is seen that our results for the perfect laminate agree well with those in Cheng et al. (2000b). The effect of interfacial imperfections on the elastic field is similar to that reported for the elastic plate (Chen et al., 2003), although it is less significant because of the relatively small values of R assumed in this paper. Hence, the reader is referred to the paper of Chen et al. (2003) for related discussions. As regards the electric field, however, the effect is very significant, as shown in Tables 8, 9 and 12.

Table 8
Amplitude of electric potential $\bar{\varphi} \times 10^3$ for a three-ply ([0/90/0°]) PVDF laminate in cylindrical bending under sinusoidal mechanical load

ζ	$a/h = 4$				$a/h = 10$			
	$R = 0.0$	$R = 0.2$	$R = 0.4$	$R = 0.6$	$R = 0.0$	$R = 0.2$	$R = 0.4$	$R = 0.6$
0	0	0	0	0	0	0	0	0
0.1	1.397073	3.490903	19.35737	−10.42074	1.975772	2.826462	8.749449	−3.137531
0.2	2.416957	6.615673	38.45022	−21.30444	3.458134	5.158595	17.00909	−6.779445
0.3	3.241167	9.568718	57.57177	−32.54382	4.528110	7.078254	24.86667	−10.84987
1/3	3.482146	10.52673	63.98121	−36.37336	4.802466	7.635944	27.40699	−12.29351
1/3	3.482146	0.329903	−26.43133	25.12498	4.802466	3.570761	−6.153121	13.94596
0.4	3.829353	2.123209	−13.71729	17.35940	5.265849	4.605596	−1.148123	10.98749
0.5	4.040864	4.491771	4.959642	5.445563	5.528004	5.722303	5.917716	6.114255
0.6	3.874457	6.479092	23.25214	−6.855779	5.270939	6.317346	12.45945	0.714481
2/3	3.550169	7.594892	35.28289	−15.31020	4.810431	6.423937	16.53186	−3.180923
2/3	3.550169	−3.542129	−57.04529	43.25955	4.810431	1.969969	−17.80807	21.88543
0.7	3.312052	−3.055150	−51.09874	38.97535	4.536211	1.981663	−15.81117	19.90095
0.8	2.485030	−1.734398	−33.59028	26.14239	3.465582	1.765867	−10.08390	13.70537
0.9	1.444454	−0.656999	−16.53141	13.23841	1.980682	1.132195	−4.788595	7.100574
1	0	0	0	0	0	0	0	0

Table 9
Amplitude of transverse electric displacement $-\overline{D}_3 \times 10^{10}$ for a three-ply ([0/90/0°]) PVDF laminate in cylindrical bending under sinusoidal mechanical load

ζ	$a/h = 4$				$a/h = 10$			
	$R = 0.0$	$R = 0.2$	$R = 0.4$	$R = 0.6$	$R = 0.0$	$R = 0.2$	$R = 0.4$	$R = 0.6$
0	0.023245	0.117935	0.836255	−0.512227	0.032974	0.129138	0.799788	−0.546710
0.1	0.036857	0.131869	0.852341	−0.500056	0.042968	0.139190	0.810179	−0.536967
0.2	0.067979	0.163916	0.890917	−0.473524	0.068901	0.165284	0.837281	−0.511832
0.3	0.105749	0.203159	0.941180	−0.443879	0.105291	0.201917	0.875574	−0.476855
1/3	0.118311	0.216322	0.959034	−0.434888	0.118882	0.215603	0.889957	−0.463884
0.4	0.122215	0.219793	0.958766	−0.427925	0.122971	0.219624	0.893433	−0.459280
0.5	0.128111	0.225514	0.962458	−0.420097	0.129166	0.225792	0.899307	−0.452760
0.6	0.134003	0.231798	0.970997	−0.415459	0.135358	0.232047	0.905893	−0.446784
2/3	0.137897	0.236268	0.979354	−0.414178	0.139443	0.236223	0.910636	−0.443144
0.7	0.150430	0.248156	0.986507	−0.398204	0.153013	0.249688	0.923396	−0.428983
0.8	0.188633	0.284924	1.012296	−0.351760	0.189373	0.285816	0.957874	−0.391177
0.9	0.220545	0.316056	1.037040	−0.314828	0.215306	0.311627	0.982715	−0.364333
1	0.234626	0.329901	1.048819	−0.299050	0.225307	0.321591	0.992361	−0.354016

To give a more direct impression, we depict the through-thickness distributions of electric potential and electric displacements in Fig. 2 for a four-layered rectangular laminate with the layup of [PZT-4/PVDF(90°)/PZT-4/PVDF(0°)] from the top to bottom. The plate, with $a/h = 4$ and $b/h = 6$, is subjected to a sinusoidal pressure $q = q_0 \sin(\pi\xi)\sin(\pi\eta)$ at the top surface. Open-circuit electric condition is assumed at both surfaces and $R^{(1)} = R^{(2)} = 2R^{(3)} = R$ is used in the calculation.

The results shown in Tables 8, 9 and 12 as well as in Fig. 2 indicate that the effect of interfacial imperfections should be exactly evaluated for smart structures. For example, when the smart laminate is controlled by a feed-back technology making use of the difference of electric potential between the top and bottom surfaces, the reaction may be amplified when the bonding imperfection is present, as shown in

Table 10
Amplitude of in-plane normal stress $\bar{\tau}_{11}$ for a three-ply ([0/90/0°]) PVDF laminate in cylindrical bending under sinusoidal mechanical load

ζ	$a/h = 4$				$a/h = 10$			
	$R = 0.0$	$R = 0.2$	$R = 0.4$	$R = 0.6$	$R = 0.0$	$R = 0.2$	$R = 0.4$	$R = 0.6$
0	−17.36568	−17.40433	−17.28472	−17.68833	−72.38055	−72.46749	−72.50849	−72.71039
0.1	−8.828046	−8.832835	−8.766047	−8.936150	−51.76590	−51.78613	−51.77512	−51.87367
0.2	−3.286680	−3.259867	−3.228147	−3.213225	−33.90355	−33.85823	−33.79535	−33.79434
0.3	1.157076	1.223984	1.226318	1.441079	−17.84170	−17.72853	−17.61114	−17.50908
1/3	2.659247	2.743600	2.735650	3.031578	−12.73792	−12.60101	−12.46437	−12.32738
1/3	0.306493	0.284214	0.202724	0.317746	−1.209034	−1.229249	−1.294360	−1.201775
0.4	0.193890	0.177336	0.103593	0.219545	−0.696063	−0.711148	−0.770904	−0.673779
0.5	0.039054	0.030419	−0.034307	0.086858	0.068841	0.061356	0.009323	0.113706
0.6	−0.106372	−0.107442	−0.165776	−0.034490	0.835557	0.835628	0.791014	0.903264
2/3	−0.202000	−0.197979	−0.253299	−0.112235	1.351757	1.356880	1.317081	1.434954
2/3	−3.220512	−3.332650	−3.536152	−3.434845	12.558065	12.42113	12.28420	12.14788
0.7	−1.627620	−1.713929	−1.864080	−1.801078	17.67897	17.56728	17.46004	17.33769
0.8	3.089206	3.064020	3.043990	3.007409	33.80166	33.76227	33.74053	33.65699
0.9	8.977917	9.004551	9.102612	8.963635	51.74164	51.77234	51.83423	51.78650
1	18.05565	18.14248	18.38699	18.10766	72.45481	72.55714	72.70523	72.69222

Table 11
Amplitude of in-plane normal stress $\bar{\tau}_{22}$ for a three-ply ([0/90/0°]) PVDF laminate in cylindrical bending under sinusoidal mechanical load

ζ	$a/h = 4$				$a/h = 10$			
	$R = 0.0$	$R = 0.2$	$R = 0.4$	$R = 0.6$	$R = 0.0$	$R = 0.2$	$R = 0.4$	$R = 0.6$
0	−0.268170	−0.276629	−0.334473	−0.228630	−1.112428	−1.121750	−1.178096	−1.069325
0.1	−0.129722	−0.137672	−0.196566	−0.086622	−0.790807	−0.799105	−0.854680	−0.744254
0.2	−0.027536	−0.035056	−0.095175	0.019016	−0.502504	−0.509800	−0.564662	−0.452511
0.3	0.061412	0.054373	−0.007297	0.112060	−0.235989	−0.242264	−0.296441	−0.182429
1/3	0.091334	0.084492	0.022212	0.143633	−0.150177	−0.156099	−0.210048	−0.095375
1/3	0.099809	0.091288	0.039866	0.130664	−0.142244	−0.150370	−0.195292	−0.111008
0.4	0.096902	0.089256	0.039136	0.129802	−0.045246	−0.052577	−0.096651	−0.011706
0.5	0.094564	0.088117	0.039430	0.130727	0.099632	0.093479	0.050611	0.136656
0.6	0.093651	0.088327	0.040519	0.133484	0.244780	0.239794	0.198063	0.285348
2/3	0.093309	0.088727	0.041226	0.135922	0.342259	0.338051	0.297044	0.385239
2/3	0.076577	0.066536	0.001069	0.119317	0.324835	0.314670	0.256482	0.366921
0.7	0.107869	0.098271	0.034055	0.150874	0.410898	0.401126	0.343456	0.453978
0.8	0.201234	0.192735	0.131640	0.244858	0.678327	0.669689	0.613486	0.724298
0.9	0.309182	0.301615	0.243102	0.353424	0.967821	0.960281	0.905465	1.016648
1	0.456170	0.449586	0.393607	0.501305	1.290955	1.284524	1.231067	1.342725

Fig. 2(a). This property can be either beneficial or harmful to the practical structures, depending on the control strategy and the method.

Finally, we give the results of a rectangular laminated PVDF piezoelectric plate with a uniform imperfection $R = 0.6$ in Table 13. All parameters are identical to that as considered in Tables 4–12, except that the laminate is not in a state of cylindrical bending and the load is $q = q_0 \sin(\pi\xi)\sin(\pi\eta)$. Just as the dynamic case, Table 13 shows that when b/a of the rectangular laminate increases, the results converge rapidly to that of the cylindrical bending problem as given in Tables 4–12. It is further shown

Table 12
Amplitude of in-plane electric displacement $-\overline{D}_1 \times 10^{10}$ for a three-ply ([0/90/0°]) PVDF laminate in cylindrical bending under sinusoidal mechanical load

ζ	$a/h = 4$				$a/h = 10$			
	$R = 0.0$	$R = 0.2$	$R = 0.4$	$R = 0.6$	$R = 0.0$	$R = 0.2$	$R = 0.4$	$R = 0.6$
0	0	0	0	0	0	0	0	0
0.1	0.312219	0.320280	0.375318	0.274649	0.602823	0.606406	0.627915	0.586479
0.2	0.457992	0.473386	0.584859	0.377898	1.019242	1.025770	1.068305	0.984408
0.3	0.485993	0.507966	0.677352	0.358199	1.271396	1.280228	1.343316	1.215900
1/3	0.471585	0.495539	0.684610	0.326480	1.321488	1.330940	1.400772	1.258601
1/3	0.074235	0.063528	−0.026194	0.146200	0.193942	0.189731	0.157113	0.224256
0.4	0.074845	0.069001	0.015855	0.119725	0.196321	0.194031	0.174703	0.215216
0.5	0.075171	0.076559	0.078004	0.079510	0.197608	0.198181	0.198758	0.199338
0.6	0.074729	0.083312	0.139313	0.038419	0.196157	0.199575	0.220039	0.180670
2/3	0.073985	0.087366	0.179878	0.010397	0.193663	0.198970	0.232691	0.166660
2/3	0.468342	0.442009	0.250564	0.606329	1.319278	1.308504	1.237353	1.378206
0.7	0.486902	0.463979	0.293644	0.611847	1.269737	1.260394	1.196796	1.323702
0.8	0.466992	0.453122	0.343164	0.551630	1.018869	1.013334	0.971792	1.056680
0.9	0.321970	0.315722	0.262487	0.364949	0.603063	0.600641	0.580292	0.622886
1	0	0	0	0	0	0	0	0

that, when $b/a = 5$, although the cylindrical bending assumption can be adopted for the determination of plate deflection, it becomes completely unsuitable for calculating the stress component σ_y. This is identical to that observed for the elastic plate (Chen et al., 2003). It is also not very accurate to predict the response of electric potential based on the assumption of cylindrical bending for a rectangular laminate with $b/a = 5$.

6. Conclusion

State-space formulations are established for analyzing the bending and free vibration problems of simply-supported laminated orthotropic piezoelectric rectangular plates. The bonding between any two adjacent layers can be either perfect or imperfect, which can be represented in a unified model of the general spring layer, in which the relation between the electric potential and electric displacement in Fan and Sze (2001) is adopted. The analysis is directly based on the three-dimensional equations of an orthotropic piezoelectric medium, without introducing any assumptions on the elastic and electric fields. Therefore, the results presented in this paper are believed to be especially valuable for further studies based on various two-dimensional approximate theories or numerical methods.

In this paper, attention is only paid to the effect of bonding imperfections on the dynamic and static behavior of laminated piezoelectric plates. A complete research should necessarily take account of the mechanism of imperfect bonding, the determination of compliance constants in the spring layer model as well as other aspects of micromechanics. These topics are however, out of the scope of this paper, and the reader is referred to Aboudi (1987), Hashin (1990) and Fan and Sze (2001), for example, for the study in this respect.

It should be pointed out that the spring layer model is only correct within the context of delamination (shear slip) initiation and on the initial growth response of the delamination (shear slip). For more general cases, non-linear interfacial constitutive relations should be developed and utilized (Williams and Addessio, 1997). However, the solution presented in the paper can be regarded as a starting point for succeeding analysis.

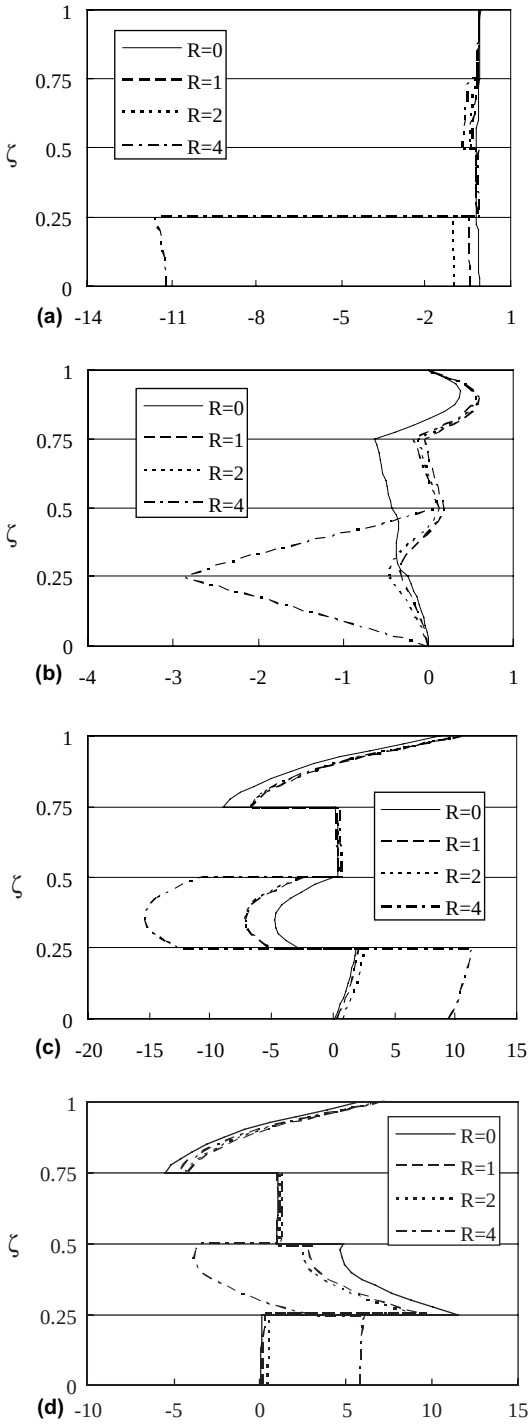

Fig. 2. Distributions of normalized electric fields along the thickness direction in a four-layered piezoelectric laminate [PZT-4/PVDF(90°)/PZT-4/PVDF(0°)]: (a) $\phi(a/2,b/2,z)\sqrt{c_{11}^{(1)}\varepsilon_{33}^{(1)}}/(hq_0)$; (b) $-D_z(a/2,b/2,z)\sqrt{c_{11}^{(1)}/\varepsilon_{33}^{(1)}}/q_0$; (c) $D_x(0,b/2,z)\sqrt{c_{11}^{(1)}/\varepsilon_{33}^{(1)}}/q_0$; (d) $D_y(a/2,0,z)\sqrt{c_{11}^{(1)}/\varepsilon_{33}^{(1)}}/q_0$.

Table 13
Amplitude of physical quantities at $\zeta = 0.5$ for a three-ply ([0/90/0°]) PVDF rectangular laminate under sinusoidal mechanical load ($R = 0.6$)

a/h	Quantity	$b/h = 4$	$b/h = 10$	$b/h = 20$	$b/h = 50$	$b/h = 100$	$b/h = 500$
4	$\bar{u}_1 \times 10^{10}$	0.006012	0.006406	0.006592	0.006728	0.006758	0.006768
	$\bar{u}_3 \times 10^{10}$	1.209096	1.823216	1.893543	1.909291	1.911371	1.912027
	$\bar{\tau}_{13}$	0.958215	1.408143	1.454453	1.464108	1.465346	1.465735
	$\bar{\tau}_{33}$	0.494647	0.499263	0.499920	0.500096	0.500121	0.500128
	$\bar{\phi} \times 10^3$	12.33100	7.123832	5.882902	5.516201	5.463245	5.446270
	$-\overline{D}_3 \times 10^{10}$	−0.384767	−0.412157	−0.417392	−0.419565	−0.419958	−0.420091
	$\bar{\tau}_{11}$	0.083829	0.085224	0.086039	0.086669	0.086807	0.086855
	$\bar{\tau}_{22}$	−0.165119	−0.094472	0.010458	0.102537	0.123178	0.130418
	$-\overline{D}_1 \times 10^{10}$	0.081218	0.082693	0.080495	0.079677	0.079552	0.079512
10	$\bar{u}_1 \times 10^{10}$	0.002543	0.003079	0.003217	0.003370	0.003448	0.003486
	$\bar{u}_3 \times 10^{10}$	1.307317	7.112815	9.163009	9.570977	9.617142	9.631190
	$\bar{\tau}_{13}$	0.732875	3.339580	4.129365	4.258685	4.271242	4.274914
	$\bar{\tau}_{33}$	0.495220	0.499560	0.500191	0.500366	0.500390	0.500398
	$\bar{\phi} \times 10^3$	10.28846	11.91559	8.142392	6.461406	6.201763	6.117765
	$-\overline{D}_3 \times 10^{10}$	−0.412860	−0.442887	−0.448063	−0.451025	−0.452183	−0.452734
	$\bar{\tau}_{11}$	0.111312	0.110992	0.111286	0.112543	0.113302	0.113688
	$\bar{\tau}_{22}$	−0.186685	−0.171192	−0.122303	0.014415	0.094300	0.134723
	$-\overline{D}_1 \times 10^{10}$	0.064976	0.179518	0.200000	0.199810	0.199470	0.199344

Acknowledgements

The work was supported by the National Natural Science Foundation of China (No. 10372088). One of the authors (CWQ) would like to express his sincere thanks to Professor Paul Heyliger for his helpful discussion. The help from two anonymous reviewers are also acknowledged.

Appendix A

The operator matrix $\mathbf{M}$ is defined as follows:

$$\mathbf{M} = \begin{bmatrix} \mathbf{0} & \mathbf{M_1} \\ \mathbf{M_2} & \mathbf{0} \end{bmatrix},$$

$$\mathbf{M_1} = \begin{bmatrix} \frac{1}{c_{55}} & 0 & -\frac{\partial}{\partial x} & -\frac{e_{15}}{c_{55}}\frac{\partial}{\partial x} \\ & \frac{1}{c_{44}} & -\frac{\partial}{\partial y} & -\frac{e_{24}}{c_{44}}\frac{\partial}{\partial y} \\ & & \rho\frac{\partial^2}{\partial t^2} & 0 \\ \text{sym.} & & & k_4\frac{\partial^2}{\partial x^2} + k_5\frac{\partial^2}{\partial y^2} \end{bmatrix},$$

$$\mathbf{M_2} = \begin{bmatrix} \rho\frac{\partial^2}{\partial t^2} - k_1\frac{\partial^2}{\partial x^2} - c_{66}\frac{\partial^2}{\partial y^2} & -(k_3 + c_{66})\frac{\partial^2}{\partial x \partial y} & -\beta_1\frac{\partial}{\partial x} & -\beta_2\frac{\partial}{\partial x} \\ & \rho\frac{\partial^2}{\partial t^2} - c_{66}\frac{\partial^2}{\partial x^2} - k_2\frac{\partial^2}{\partial y^2} & -\beta_3\frac{\partial}{\partial y} & -\beta_4\frac{\partial}{\partial y} \\ & & \frac{\varepsilon_{33}}{\alpha} & \frac{e_{33}}{\alpha} \\ \text{sym.} & & & -\frac{c_{33}}{\alpha} \end{bmatrix}, \tag{A.1}$$

where

$$\begin{aligned}
&\alpha = c_{33}\varepsilon_{33} + e_{33}^2, \quad \beta_1 = (c_{13}\varepsilon_{33} + e_{31}e_{33})/\alpha, \quad \beta_2 = (c_{13}e_{33} - c_{33}e_{31})/\alpha,\\
&\beta_3 = (c_{23}\varepsilon_{33} + e_{32}e_{33})/\alpha, \quad \beta_4 = (c_{23}e_{33} - c_{33}e_{32})/\alpha,\\
&k_1 = c_{11} - c_{13}\beta_1 - e_{31}\beta_2, \quad k_2 = c_{22} - c_{23}\beta_3 - e_{32}\beta_4,\\
&k_3 = c_{12} - c_{13}\beta_3 - e_{31}\beta_4 = c_{12} - c_{23}\beta_1 - e_{32}\beta_2,\\
&k_4 = \varepsilon_{11} + e_{15}^2/c_{55}, \quad k_5 = \varepsilon_{22} + e_{24}^2/c_{44}.
\end{aligned} \tag{A.2}$$

The five induced variables are determined by

$$[\sigma_x, \sigma_y, \tau_{xy}, D_x, D_y]^{\mathrm{T}} = \mathbf{N}[u, v, \sigma_z, D_z, \tau_{xz}, \tau_{yz}, w, \phi]^{\mathrm{T}}, \tag{A.3}$$

where,

$$\mathbf{N} = \begin{bmatrix} \mathbf{N_1} & \mathbf{0} \\ \mathbf{0} & \mathbf{N_2} \end{bmatrix},$$

$$\mathbf{N_1} = \begin{bmatrix} k_1\frac{\partial}{\partial x} & k_3\frac{\partial}{\partial y} & \beta_1 & \beta_2 \\ k_3\frac{\partial}{\partial x} & k_2\frac{\partial}{\partial y} & \beta_3 & \beta_4 \\ c_{66}\frac{\partial}{\partial y} & c_{66}\frac{\partial}{\partial x} & 0 & 0 \end{bmatrix}, \quad \mathbf{N_2} = \begin{bmatrix} \frac{e_{15}}{c_{55}} & 0 & 0 & -k_4\frac{\partial}{\partial x} \\ 0 & \frac{e_{24}}{c_{44}} & 0 & -k_5\frac{\partial}{\partial y} \end{bmatrix}. \tag{A.4}$$

The dimensionless constant matrix $\overline{\mathbf{M}}$ is given by

$$\overline{\mathbf{M}} = \begin{bmatrix} \mathbf{0} & \overline{\mathbf{M}}_\mathbf{1} \\ \overline{\mathbf{M}}_\mathbf{2} & \mathbf{0} \end{bmatrix}, \tag{A.5}$$

$$\overline{\mathbf{M}}_\mathbf{1} = \begin{bmatrix} \frac{c_{11}^{(1)}}{c_{55}} & 0 & -t_1 & -\frac{e_{15}}{c_{55}}\sqrt{\frac{c_{11}^{(1)}}{\varepsilon_{33}^{(1)}}}t_1 \\ & \frac{c_{11}^{(1)}}{c_{44}} & -t_2 & -\frac{e_{24}}{c_{44}}\sqrt{\frac{c_{11}^{(1)}}{\varepsilon_{33}^{(1)}}}t_2 \\ & & -\kappa & 0 \\ \text{sym.} & & & \frac{1}{\varepsilon_{33}^{(1)}}(k_4t_1^2 + k_5t_2^2) \end{bmatrix},$$

$$\overline{\mathbf{M}}_\mathbf{2} = \begin{bmatrix} \kappa + \frac{k_1}{c_{11}^{(1)}}t_1^2 + \frac{c_{66}}{c_{11}^{(1)}}t_2^2 & \frac{c_{66}+k_3}{c_{11}^{(1)}}t_1t_2 & \beta_1t_1 & \beta_2\sqrt{\frac{\varepsilon_{33}^{(1)}}{c_{11}^{(1)}}}t_1 \\ & \kappa + \frac{c_{66}}{c_{11}^{(1)}}t_1^2 + \frac{k_2}{c_{11}^{(1)}}t_2^2 & \beta_3t_2 & \beta_4\sqrt{\frac{\varepsilon_{33}^{(1)}}{c_{11}^{(1)}}}t_2 \\ & & -\frac{\varepsilon_{33}c_{11}^{(1)}}{\alpha} & -\frac{e_{33}\sqrt{\varepsilon_{33}^{(1)}c_{11}^{(1)}}}{\alpha} \\ \text{sym.} & & & \frac{c_{33}\varepsilon_{33}^{(1)}}{\alpha} \end{bmatrix},$$

where $t_1 = m\pi h/a$, $t_2 = n\pi h/b$, $\kappa = -\Omega^2\rho/\rho^{(1)}$, and $\Omega = \omega h\sqrt{\rho^{(1)}/c_{11}^{(1)}}$ is the dimensionless frequency.

The state equation for cylindrical bending problem can be derived as

$$\frac{\partial}{\partial z}\begin{Bmatrix} u \\ \sigma_z \\ D_z \\ \tau_{xz} \\ w \\ \phi \end{Bmatrix} = \begin{bmatrix} & & & \frac{1}{c_{55}} & -\frac{\partial}{\partial x} & -\frac{e_{15}}{c_{55}}\frac{\partial}{\partial x} \\ & \mathbf{0} & & & \rho\frac{\partial^2}{\partial t^2} & 0 \\ & & & \text{sym.} & & k_4\frac{\partial^2}{\partial x^2} \\ \rho\frac{\partial^2}{\partial t^2} - k_1\frac{\partial^2}{\partial x^2} & -\beta_1\frac{\partial}{\partial x} & -\beta_2\frac{\partial}{\partial x} & & & \\ & \frac{\varepsilon_{33}}{\alpha} & \frac{e_{33}}{\alpha} & & \mathbf{0} & \\ \text{sym.} & & -\frac{c_{33}}{\alpha} & & & \end{bmatrix}\begin{Bmatrix} u \\ \sigma_z \\ D_z \\ \tau_{xz} \\ w \\ \phi \end{Bmatrix}. \tag{A.6}$$

References

Aboudi, J., 1987. Damage in composites-modelling of imperfect bonding. Comp. Sci. Tech. 28, 103–128.

Altay, G.A., Dökmeci, M.C., 2003. Some comments on the higher order theories of piezoelectric, piezothermoelastic and thermopizoelectric rods and shells. Int. J. Solids Struct. 40, 4699–4706.

Bahar, L.Y., 1975. A state space approach to elasticity. J. Franklin Inst. 299, 33–41.

Chen, W.Q., Cai, J.B., Ye, G.R., 2003. Exact solutions of cross-ply laminates with bonding imperfections. AIAA J. 41, 2244–2250.

Chen, W.Q., Ding, H.J., Xu, R.Q., 2001. Three-dimensional static analysis of multi-layered piezoelectric hollow spheres via the state space method. Int. J. Solids Struct. 38, 4921–4936.

Chen, W.Q., Lee, K.Y., 2004. Three-dimensional exact analysis of angle-ply laminates in cylindrical bending with interfacial damage via state-space method. Compos. Struct. 64, 275–283.

Chen, W.Q., Liang, J., Ding, H.J., 1997. Three dimensional analysis of bending problem of thick piezoelectric composite rectangular plates. Acta Mater. Compos. Sinica 14, 108–115 (in Chinese).

Chen, W.Q., Wang, Y.F., Cai, J.B., Ye, G.R., 2004a. Three-dimensional analysis of cross-ply laminated cylindrical panels with weak interfaces. Int. J. Solids Struct. 41, 2429–2446.

Chen, W.Q., Xu, R.Q., Ding, H.J., 1998. On free vibration of a piezoelectric composite rectangular plate. J. Sound Vib. 218, 741–748.

Chen, W.Q., Ying, J., Cai, J.B., Ye, G.R., 2004b. Benchmark solution of laminated beams with bonding imperfections. AIAA J. 42, 426–429.

Cheng, Z.Q., Jemah, A.K., Williams, F.W., 1996a. Theory for multilayered anisotropic plates with weakened interfaces. J. Appl. Mech. 63, 1019–1026.

Cheng, Z.Q., Kennedy, D., Williams, F.W., 1996b. Effect of interfacial imperfection on buckling and bending behavior of composite laminates. AIAA J. 34, 2590–2595.

Cheng, Z.Q., He, L.H., Kitipornchai, S., 2000a. Influence of imperfect interfaces on bending and vibration of laminated composite shells. Int. J. Solids Struct. 37, 2127–2150.

Cheng, Z.Q., Lim, C.W., Kitipornchai, S., 2000b. Three-dimensional asymptotic approach to inhomogeneous and laminated piezoelectric plates. Int. J. Solids Struct. 37, 3153–3175.

Ding, H.J., Chen, W.Q., 2001. Three Dimensional Problems of Piezoelasticity. Nova Science Publishers, New York.

Ding, H.J., Xu, R.Q., Chi, Y.W., Chen, W.Q., 1999. Free axisymmetric vibration of transversely isotropic piezoelectric circular plates. Int. J. Solids Struct. 36, 4629–4652.

Fan, H., Sze, K.Y., 2001. A micro-mechanics model for imperfect interface in dielectric materials. Mech. Mater. 33, 363–373.

Fernandes, A., Pouget, J., 2002. An accurate modeling of piezoelectric multi-layer plates. Europ. J. Mech. A/Solids 21, 629–651.

Hashin, Z., 1990. Thermoelastic properties of fiber composites with imperfect interface. Mech. Mater. 8, 333–348.

Heyliger, P., 2003. Private communication.

Heyliger, P., Saravanos, D.A., 1995. Exact free vibration analysis of laminated plates with embedded piezoelectric layers. J. Acoust. Soc. Amer. 98, 1547–1557.

Icardi, U., Di Sciuva, M., Librescu, L., 2000. Dynamic response of adaptive cross-ply cantilevers featuring interlaminar bonding imperfections. AIAA J. 38, 499–506.

Lee, J.S., Jiang, L.Z., 1996. Exact electroelastic analysis of piezoelectric laminate via state space approach. Int. J. Solids Struct. 33, 977–990.

Librescu, L., Schmidt, R., 2001. A general linear theory of laminated composite shells featuring interlaminar bonding imperfections. Int. J. Solids Struct. 38, 3355–3375.

Liu, D., Xu, L., Lu, X., 1994. Stress analysis of imperfect composite laminates with an interlaminar bonding theory. Int. J. Numer. Meth. Eng. 37, 2819–2839.

Rogacheva, N.N., 1994. The Theory of Piezoelectric Shells and Plates. CRC Press, Boca Raton, FL.

Seeley, C.E., Chattopadhyay, A., 1999. Modeling of adaptive composites including debonding. Int. J. Solids Struct. 36, 1823–1843.

Shu, X.P., Soldatos, K.P., 2001. An accurate delamination model for weakly bonded laminates subjected to different sets of edge boundary conditions. Int. J. Mech. Sci. 43, 935–959.

Sosa, H., 1992. On the modeling of piezoelectric laminated structures. Mech. Res. Commun. 19, 541–546.

Tani, J., Takagi, T., Qiu, J., 1998. Intelligent material systems: application of functional materials. Appl. Mech. Rev. 51, 505–521.

Tzou, H.S., 1993. Piezoelectric Shells: Distributed Sensing and Control of Continua. Kluwer Academic Publications, Dordrecht.

Wang, J., Yang, J.S., 2000. Higher-order theories of piezoelectric plates and applications. Appl. Mech. Rev. 53, 87–99.

Wang, X., Zhong, Z., 2003. Three-dimensional solution of smart laminated anisotropic circular cylindrical shells with imperfect bonding. Int. J. Solids Struct. 40, 5901–5921.

Williams, T.O., Addessio, F.L., 1997. A general theory for laminate plates with delaminations. Int. J. Solids Struct. 34, 2003–2024.

Yue, Z.Q., Yin, J.H., 1998. Backward transfer-matrix method for elastic analysis of layered solids with imperfect bonding. J. Elast. 50, 109–128.

Zou, Y., Tong, L., Steven, G.P., 2000. Vibration-based model-dependent damage (delamination) identification and health monitoring for composite structures—a review. J. Sound Vib. 230, 357–378.